

## ARTICLE OPEN



# Tripartite motif 25 ameliorates doxorubicin-induced cardiotoxicity by degrading p85 $\alpha$

Yihui Shen<sup>1,2,6</sup>, Hui Zhang<sup>1,2,6</sup>, Yangyue Ni<sup>3,6</sup>, Xuejun Wang<sup>1,2</sup>, Yifan Chen<sup>2</sup>, Jiahui Chen<sup>2</sup>, Yan Wang<sup>4</sup>, Jinyi Lin<sup>2</sup>, Yuchen Xu<sup>2</sup>, Jian-Yuan Zhao<sup>5</sup> and Leilei Cheng<sup>1,2</sup>

© The Author(s) 2022

Doxorubicin (DOX)-based chemotherapy is widely used to treat malignant tumors; however, the cardiotoxicity induced by DOX restricts its clinical usage. A therapeutic dose of DOX can activate ubiquitin-proteasome system. However, whether and how ubiquitin-proteasome system brings out DOX-induced cardiotoxicity remains to be investigated. Here we conducted a proteomics analysis of a DOX-induced cardiotoxicity model to screen the potentially ubiquitination-related molecules. Dysregulated TRIM25 was found to contribute to the cardiotoxicity. In vivo and in vitro cardiotoxicity experiments revealed that TRIM25 ameliorated DOX-induced cardiotoxicity. Electron microscopy and endoplasmic reticulum stress markers revealed that TRIM25 mitigated endoplasmic reticulum stress and apoptosis in DOX-induced cardiomyocytes. Mechanistically, the Co-immunoprecipitation assays and CHX pulse-chase experiment determined that TRIM25 affected p85 $\alpha$  stability and promoted its ubiquitination and degradation. This leads to increase of nuclear translocation of XBP-1s, which mitigates endoplasmic reticulum stress. These findings reveal that TRIM25 may have a therapeutic role for DOX-induced cardiotoxicity.

*Cell Death and Disease* (2022)13:643; <https://doi.org/10.1038/s41419-022-05100-4>

## INTRODUCTION

Anthracycline-based chemotherapy has been widely used to treat malignant tumors for the past eight decades. Unfortunately, based on previous studies, anthracyclines such as doxorubicin (DOX) can result in cardiotoxicity progressing to heart failure [1, 2]. A recent multicenter cohort study also showed that patients with cancer have a substantially increased risk of death caused by cardiovascular diseases even 40 years after initial chemotherapy treatment [3]. Several mechanisms may be responsible for DOX-induced cardiotoxicity, such as an excess of reactive oxygen species (ROS), mitochondrial dysfunction, and autophagy. However, optimal interventions for DOX-induced cardiotoxicity are yet to be fully determined [4, 5]; thus, further research is warranted to better understand the mechanism of DOX-induced cardiotoxicity.

Various studies have indicated that protein degradation by the ubiquitin-proteasome system regulates many fundamental biological processes in cardiovascular development and disease [6, 7]. Dysfunctional expression of ubiquitin E3 ligases, which mainly determines the specificity and rate-limiting step of ubiquitination, plays an essential role in the pathological processes of various diseases [8, 9]. Regulating the levels of ubiquitin E3 ligases has been proven to be able to treat many cardiovascular diseases, such as cardiac hypertrophy, valve calcification, and pulmonary arterial hypertension [10–12].

Recent studies have revealed that a therapeutic dose of DOX can activate ubiquitin-proteasome system-mediated proteolysis in cardiomyocytes [13]. The levels of some ubiquitin E3 ligases, such as atrogin-1, were increased in response to DOX treatment [14, 15]. Given that the expression patterns of ubiquitin E3 ligases in DOX-induced cardiotoxicity are yet to be elucidated, we conducted proteomics analysis of a DOX-induced cardiotoxicity model. Among the identified ubiquitin E3 ligases, TRIM25 is one of the tripartite motif-containing (TRIM) family proteins, which contain a RING finger domain followed by one or two B-Box domains and a coiled-coil domain [16]. Various studies have reported that TRIM family proteins play an indispensable role in regulating the antiviral innate immune response, metabolism, etc., via their ubiquitin ligase activity. Disorders of TRIM16 are reportedly involved in lipid metabolism in hepatocytes [17]. For example, overexpression of TRIM16 controls hepatic lipid accumulation and inflammation through the regulation of p-TAK1. Moreover, TRIM25 is essential for RIG-I ubiquitination, which is crucial for the RIG-I-mediated interferon- $\beta$  production [18]. However, the role of TRIM25 in cardiovascular disease remains unknown.

Thus, we aimed to identify the expression patterns of ubiquitin E3 ligase in DOX-induced cardiotoxicity, and to investigate the role of TRIM25 in DOX-induced cardiotoxicity as well as its potential molecular mechanisms.

<sup>1</sup>Department of Echocardiography, Zhongshan Hospital, Fudan University, Shanghai Institute of Cardiovascular Diseases, Shanghai Institute of Medical Imaging, 180 Fenglin Road, Shanghai, China. <sup>2</sup>Department of Cardiology, Zhongshan Hospital, Fudan University, Shanghai Institute of Cardiovascular Diseases, 180 Fenglin Road, Shanghai, China. <sup>3</sup>State Key Laboratory of Cell Biology, Center for Excellence in Molecular Cell Science, Shanghai Institute of Biochemistry and Cell Biology, Chinese Academy of Sciences, University of Chinese Academy of Sciences, Shanghai, China. <sup>4</sup>Department of Medical Oncology, Zhongshan Hospital, Fudan University, Shanghai 200032, China. <sup>5</sup>Institute for Developmental and Regenerative Cardiovascular Medicine, MOE-Shanghai Key Laboratory of Children's Environmental Health, Xinhua Hospital, Shanghai Jiao Tong University School of Medicine, Shanghai 200092, China. <sup>6</sup>These authors contributed equally: Yihui Shen, Hui Zhang, Yangyue Ni. ✉email: zhaoyj@vip.163.com; cheng.leilei@zs-hospital.sh.cn Edited by Professor Sergio Lavandro

Received: 9 February 2022 Revised: 8 July 2022 Accepted: 13 July 2022

Published online: 23 July 2022

## MATERIAL AND METHODS

### Mice

Animals were housed in a specific pathogen-free facility according to the guidelines of the Care and Use of Laboratory Animals (published by the national institutes of health, NIH publication no.86-23, revised 1996). The experiments were approved by the animal care and use committee of Zhongshan Hospital Research Ethics. Adult male C57BL/6 mice (8–10 weeks old, weighing 20–24 g), purchased from Shanghai Laboratory Animal Center of Fudan university (Shanghai, China) were randomly assigned to each group for studies on Dox-induced cardiotoxicity ( $n = 7–10$ ). Sample size was determined by power calculations based on data from preliminary experiments with an  $\alpha$  level of 0.05 and power of 0.80, a minimum number of 5 mice per group was required. A simple and free online randomization tool was performed by GraphPad (<https://www.graphpad.com/quickcalcs/randomize1.cfm>). After the randomized allocation of animals to the treatments, animals, samples, and treatments are coded and recorded until the data are analyzed.

### In vivo treatments

To generate DOX-induced cardiotoxicity, male C57/B6 mice were administered weekly intraperitoneal injections of DOX (5 mg/kg on days 0, 7, 14 and 21) for 4 weeks and heart function was assessed by echocardiography, 8 weeks after the first injection of DOX (cumulating dose 20 mg/kg of body weight). DOX was freshly dissolved in 0.9% NaCl (1 mL/kg). The saline group received an equal volume of fluid in the same period.

To investigate ER stress in vivo, mice were treated i.p. with a single injection of 5 mg/kg DOX. Mice were sacrificed and hearts collected for transmission electron microscopy analysis 4 weeks and 8 weeks after dox injection separately.

To determine the ability of anti-ER stress chemical agent TUDCA (Tauroursodeoxycholic Acid) to relieve DOX-induced cardiotoxicity in vivo, mice were treated i.p. with 300 mg/kg TUDCA or vehicle (DMSO) daily for 4 weeks, commencing on the one day before DOX treatment [19].

To examine the effect of TRIM25 on ER stress responses in vivo, mice were treated i.p. with 2 mg/kg TM (Tunicamycin), and 1 mg/kg TM (Tunicamycin) or vehicle (DMSO) 1 h before injection of DOX (on days 0, 7, 14 and 21). Given that the mice treated with 2 mg/kg TM (Tunicamycin) all died within 1 weeks, the mice treated with 1 mg/kg TM were used for later assessment.

Cardiomyocyte-restricted, genetic overexpressed of TRIM25 was performed by i.v. injection of 10  $\mu$ l of AAV9-cTNT-GFP-TRIM25 ( $1 \times 10^{13}$  v.g/ml; Genechem, shanghai, China) in 8-week-old C57/B6 mice (cumulating dose  $1 \times 10^{11}$  v.g per mouse). Similarly, to specifically overexpress p85 $\alpha$  in the myocardium, 8-week-old C57/B6 mice received a single intravenous injection of 20  $\mu$ l of AAV9-cTNT-GFP-p85 $\alpha$  ( $0.5 \times 10^{13}$  v.g/ml; Genechem, shanghai, China) (cumulating dose  $1 \times 10^{11}$  v.g per mouse). Dox was injected 4 weeks after the injection of AAV9.

### Echocardiography and measurements

Transthoracic echocardiography was performed using a 30 MHz high-frequency scan probe (VisualSonics Vevo2100; VisualSonics, Toronto, Canada) 8 weeks after the first injection of DOX. Anesthesia was induced by putting the mice in an induction chamber using 2% isoflurane (HEBEL YIPIN Pharmaceutical, Shanghai, China) and 2 L/min 100% oxygen for 1–2 min. Next, mice were placed on a constant temperature table in the supine position. M-mode images were recorded when the heart rate (HR) of the mice was maintained at 350–550 bpm. Heart rate (HR), left ventricular ejection fraction (LVEF), cardiac output (CO), fractional shortening (FS), left ventricular end-diastolic dimension (LVEDD), and left ventricular end-systolic dimension (LVESD) were measured as previously described [1]. All measurements were averaged for 3 consecutive cardiac cycles and were carried out by one experienced technician who was blinded to the experimental group identities.

### Isolation of neonatal mouse ventricular cardiomyocytes (NMVMs)

Neonatal mouse ventricular cardiomyocytes (NMVMs) were isolated and cultured as previously described [20]. Briefly, hearts of 1- to 3-day-old pups were dissected and atria were removed. Ventricles were minced and digested with repeatedly with 0.25% trypsin at 37 °C for 30 s to 1 min per cycle. When the cell supernatant became cloudy, the supernatant was neutralized by culture solution containing 10% serum. After 20–30 cycles of digestion, supernatant containing isolated cells were collected. The

obtained cells were centrifuged 5 min at 800 rpm to separate non-myocardial cells and cultured at 37 °C in a humidified 5% CO<sub>2</sub> incubator. One hour later, the supernatant containing suspended cardiomyocytes was transferred into other plates to reduce fibroblast contamination. Next, cell supernatant was passed through a 100  $\mu$ m filter. Cardiomyocytes were cultured in Dulbecco's modified Eagle's medium (DMEM) High Glucose, supplemented with 10% Fetal Bovine Serum (FBS), and 5 mM penicillin/streptomycin (Gibco, Carlsbad, CA) for 2–3 days. Cardiomyocytes were used in experiments after the cells formed a confluent monolayer and contracted in synchrony.

### Cell cultures

The mouse cardiac muscle cell line HL-1 and rat cardiomyoblast cell line H9C2 were purchased from the Cell Bank of the Chinese Academy of Science (Shanghai, China) and were cultured in DMEM (Dulbecco's Modified Eagle Medium) High Glucose (Gibco, Shanghai, China) supplemented with 10% FBS, 5 mM penicillin/streptomycin (Gibco, Shanghai, China). Human embryonic kidney cells 293T (HEK-293T) was kindly provided by Doc. Zhiyuan Zhang (Dept. of General Surgery, Zhongshan Hospital, Fudan University, Shanghai, China) and cultured in DMEM High Glucose supplemented with 10%FBS, 5 mM penicillin/streptomycin. Cells were passaged at 70–80% confluence by dissociation from plates using Trypsin-EDTA. All cells were incubated under 5% CO<sub>2</sub> at 37 °C.

To avoid the effect of high glucose on ER stress pathway, we used DMEM Low Glucose in DOX -induced ER stress model in vitro.

### Cell transfection and virus infection

To study the effect of TRIM25 on the HL-1 cells' viability, HL-1 cells were infected with shRNA -TRIM25, for 24 h using Lipofectamine™ 3000 Transfection Reagent (#L3000015, ThermoFisher, Shanghai, China) according to the manufacturer's Reagent protocol.

Expression plasmids encoding p85 $\alpha$  (encoded by Pik3r1), ubiquitin (Ub), TRIM25-WT, TRIM25-2EA, p85 $\alpha$ -K506R, and p85 $\alpha$ -K511R (p85 $\alpha$  mutants with lys506 and lys511 changed into Arg were termed as K506R and K511R) were purchased from Genechem (Genechem, Shanghai, China). All plasmids were transfected with Lipofectamine™ 3000 Transfection Reagent (#L3000015, ThermoFisher, Shanghai, China) according to the protocol.

Adenovirus-driven ectopic expressing TRIM25 was achieved by infecting cultured cells at 50 MOI.

The reagents used and their commercial sources were indicated as follows: Doxorubicin (DOX) (selleckchem), cycloheximide (CHX) (selleckchem), MG132 (selleckchem), Tauroursodeoxycholic Acid (TUDCA) (selleckchem), Tunicamycin (TM) (MedChemExpress, Shanghai, China) and protein G agarose beads (#16–266, Merck Millipore, USA).

### Transmission electron microscopy analysis

Hearts samples were harvested from mice. 1 mm<sup>3</sup> heart pieces from the left ventricular wall were fixed in 1.25% glutaraldehyde (pH 7.2, Servicebio, Wuhan, China) overnight at 4 °C. Heart samples were washed in 0.1 M sodium cacodylate (3 times for 30 min), post-fixed and thin sections were imaged on a HITACHI electron microscopy (HT 7800, Japan).

### Quantitative real-time PCR

Total RNA extraction of the cells or heart tissues was extracted using RNAiso Plus (#9109, TAKARA, China) and 1  $\mu$ g RNA was reverse transcribed by the PrimeScript™ RT Master Mix (Perfect Real Time) (# RR036A, TAKARA, China). Quantitative real-time (qRT) PCR was performed by SYBR Green PCR Master Mix (Applied Biosystems, CA) in the ABI 7300 Detection System (Applied Biosystems, CA). The qRT-PCR primers sequences of the detected genes were showed in the Supplementary Table 2.

### Western blot analysis

Total proteins isolated from the left ventricle of heart tissues, NMVMs, HL-1, H9C2, and HEK-293T cells were lysated in ice-cold lysis buffer for 30 min with protease and phosphatase inhibitors (Thermo Fisher Scientific, MA, USA). The protein concentration was quantified using BCA protein assay kit (Pierce™ BCA Protein Assay Kit, Thermo Scientific, China) following the manufacturer's instructions. Protein (30  $\mu$ g/lane) was loaded on SDS-PAGE and then transferred to 0.22  $\mu$ m PVDF membranes (Merck Millipore, Billerica, MA, USA). The membranes were blocked with 5% BSA (Bovine serum albumin, Sigma, USA) for 2 h at room temperature and incubated at 4 °C overnight with primary antibodies. The primary antibodies used in this study are listed in

Supplementary Table 1. After washing with TBST (Sangon Biotech, Shanghai, China), the membranes were incubated with a horseradish peroxidase HRP-conjugated antibody #7076 S, #7074 S(1:3000, Cell Signaling Technology, USA). GAPDH or Lamin A/C was used as an internal control. The proteins were visualized using an ECL Western blotting detection system #WBKLS0500 (MILLIPORE, USA). The density of each band was quantified by densitometric analysis with ImageJ software (Image Processing and Analysis in Java, National Institutes of Health, USA).

### Morphological and histological analysis

The hearts were perfused with PBS (Phosphate Buffered Saline, Hyclone) and then isolated to measure their weight. The heart samples were fixed with 4% paraformaldehyde and embedded in paraffin. The paraffin-embedded hearts were sectioned at a thickness of 5  $\mu$ m and stained with eosin (H&E) and Masson's trichrome for the analysis of atrophy and fibrosis according to the manufacturer's recommended protocol (Servicebio Biotech, Wuhan, China). For measurements, 5 random high-power fields from 5 sections of each heart were chosen and quantified in a blinded manner. The cross-sectional area (CSA) of the cardiomyocytes and the area of the cardiac fibrosis were evaluated through morphometric analysis of the H&E-stained and Masson's trichrome sections respectively. Specimens were observed under a light microscope (400 amplification; Nikon Tokyo, Japan). The images were measured through an automated image analysis system (Image-Pro Plus 5.0).

### Tissue preparation and immunofluorescence analysis

For IF assay, the 5  $\mu$ m cryosections were fixed in 4% paraformaldehyde for 30 min and next washed in phosphate buffered saline (PBS) for 3 times. The sections were permeabilized with 0.3% Triton X-100 in PBS for 10 min and blocked with 10% normal goat serum (Beyotime, Jiangsu, China) for 1 h at RT. The slides were then incubated with primary antibodies overnight at 4 °C, followed by secondary antibodies at RT for 1 h. The images were captured using fluorescence microscope (Nikon Tokyo, Japan) or Zeiss Pascal confocal microscope (Zeiss, FV3000, Germany), quantified by ImageJ software (<https://imagej.nih.gov/ij/>).

### Evaluation of apoptosis

TUNEL labeling was conducted in accordance with the manufacturer's protocol (One Step TUNEL Apoptosis Assay Kit; Beyotime, Jiangsu, China). In brief, the paraffin-embedded slides were incubated with 50  $\mu$ l of TUNEL reaction mixture containing terminal deoxynucleotidyl transferase (TdT) and biotinylated dUTP for 1 h at 37°C. After washing with PBS three times, Hoechst 33258 was dispensed dropwise onto the slides and incubated for 5 min at the room temperature. The apoptosis-positive cells were counted in 6 randomly selected fields from each slide. The results were recorded as the ratio of TUNEL-positive nuclei/Hoechst 33258-stained nuclei and analyzed via fluorescence microscopy.

### Proteomics analysis

The samples from PBS and DOX treated HL-1 cells were added with appropriate amount of SDS cracking solution, boiling water bath for 15 min. 14000 g centrifuged for 15 min, the supernatant was removed. Carryon protein quantitative analysis by BCA method. Each sample was labelled with 100  $\mu$ g Peptide, according to TMT 6/10plex Isobaric Mass Tag Labeling kit (Thermo Fisher scientific). After that, labeled samples were separated by Easy nLC system (Thermo Fisher Scientific, Waltham, MA, USA) and processed for gradient elution by a analytical column (Thermo Fisher Scientific, Acclaim PepMap RSLC 50  $\mu$ m X 15 cm). The samples were analyzed for TMT Quantitative proteomics by Q Exactive plus Mass Spectrometer. The raw data of mass spectrometry analysis was conducted inventory identification and quantitative analysis using software Mascot 2.6 and Proteome Discoverer2.1. Proteins with a 1.2-fold change ( $\geq 1.2$  or  $\leq 0.83$ ) and corresponding adjusted  $P < 0.05$  were identified as target molecules and entered into the Database for Annotation, Visualization and Integrated Discovery (DAVID, <http://david.abcc.ncifcrf.gov>) and then subjected to Gene Ontology (GO) and Kyoto Encyclopedia of Genes and Genomes (KEGG) pathway database. The proteomics analysis was performed and analyzed by Genechem (Shanghai).

### Bioinformatics analysis

We analyzed a GEO RNA-seq dataset (GSE40289) generated from the cardiomyocytes with or without DOX treatment from mice isolated by

using a Langendorff apparatus, with the tool R language (Version 3.61) used to analyse the raw data. The lists of differentially changed ubiquitin E3 ligase in cardiomyocytes treated with DOX were shown in Supplementary Table 3. Spectrum of total ubiquitin E3 ligases were from Integrated Genomic Analysis [21].

### Identify TRIM25 and p85 $\alpha$ interaction proteins by mass spectrometry

Five 10 cm dishes HL-1/HEK293T cells were transfected with empty vectors or GV314-3Flag-p85 $\alpha$  or GV314-3Flag-TRIM25 with Lipofectamine 3000 and continued cultured for 48 h. Then cells were lysed in Co-IP buffer (50.0 mM Tris-HCl, 150.0 mM NaCl, 5.0 mM EDTA, and 1.0% NP-40 pH 7.6) supplemented with protease inhibitor cocktail (HY-K0010, MedChemExpress, China), and incubated with anti-Flag affinity gels (A4596, Sigma-Aldrich, USA) overnight at 4 °C. The immunoprecipitates were washed three times with COIP buffer. Bound proteins were analysed by immunoprecipitation-mass spectrometry.

### Co-immunoprecipitation

For co-immunoprecipitation, assays were performed as described previously [22]. Briefly, tissues/cells were homogenized in COIP buffer (50 mM Tris-HCl, 150 mM NaCl, 5 mM EDTA and 1% NP-40 pH 7.6) supplemented with protease inhibitor cocktail (MedChemExpress, Shanghai, China). Then, cell lysates were incubated and rocked with indicated antibody and Protein G agarose beads (16-266, Millipore, Shanghai, China), or affinity gels (Sigma-Aldrich, Shanghai, China) overnight at 4 °C. Proteins bound to protein G-Sepharose were washed, and denatured in 2 $\times$  SDS-PAGE loading buffer at 100 °C for 10 min. Then proteins were subjected to SDS-PAGE and analyzed by Western Blot.

### Expression and purification of recombinant proteins

Expression and purification of recombinant proteins were performed as described previously [23]. Briefly, GST- or His6 (His)-tag proteins were expressed in the BL21 (DE3) *Escherichia coli* cells. After IPTG (isopropyl  $\beta$ -D-thiogalactoside, Sigma, USA) induction, cells were pelleted, lysed and incubated with glutathione or Ni<sup>2+</sup> IDA resin to enrich the respective proteins, eluted with 40 mM reduced glutathione (GSH, Sigma) or 100 mM imidazole dissolved in Tris buffer (pH 8.0). Protein expressed as inclusion bodies was dialyzed in PBS buffer supplemented with 4 mM GSH, 0.4 mM GSSG, 0.4 M L-Arginine, 1 M Urea. The purity of recombinant protein was examined by SDS-PAGE with Coomassie blue staining and Western Blot, then aliquoted and preserved in 20% glycerol at -80 °C.

### GST pull-down assay

The pull-down assay was conducted as by the instruction (Pierce™ GST Protein Interaction Pull-Down Kit, #21516, Thermo scientific, USA). Briefly, the purified GST-p85 $\alpha$  or GST-empty (Bait Protein, approximately 150  $\mu$ g of bait protein) were added to the Pierce spin Column and incubated at 4 °C for 30 min with gentle rocking motion on a rotating platform. Next, His-TRIM25 (Prey Protein) was incubated with the GST-tagged bait protein at 4 °C for 1 h. Then the beads were washed five times with washing buffer. Next, bait-prey protein was eluted and then centrifuged at 1250 g for 30 s. The bait-prey protein was denatured at 100 °C for 10 min in 2 $\times$  SDS-PAGE loading buffer and subjected to Coomassie blue staining or western blot analysis.

### Statistical analysis

All data are expressed as the mean  $\pm$  standard error of the mean (SEM). Comparison between two groups was performed by the two-tailed Student's *t*-test. Comparisons between multiple groups were conducted using a one-way ANOVA analysis with Bonferroni's multiple comparisons test. Before using statistical analysis, Homogeneity of variance test was tested by bartlett testing. All data analysis was conducted by Prism 8.0 (GraphPad Software, CA, USA). A value of  $P < 0.05$  was considered as statistically significant. The precise *P*-value of significant changes were shown in each figure.

## RESULTS

### Expression patterns of ubiquitin E3 ligases in doxorubicin-induced cardiotoxicity

To investigate the expression profile of ubiquitin E3 ligases in cardiomyocytes in response to DOX, we performed tandem mass

tag proteomics of a DOX-induced cardiotoxicity cell-based model, which consisted of HL-1 mouse cardiomyocytes treated with DOX for 16 h. Furthermore, we searched an RNA-seq (GSE40289) of a tissue-based model to identify stable ubiquitination-associated candidate molecules (Fig. 1a). A total of 6326 proteins were detected in the proteomics results, and 1858 proteins were differentially expressed between DOX-treated and normal cardiomyocytes. Among these, 231 were significantly upregulated in DOX-treated cardiomyocytes whereas 167 were downregulated (fold change >1.2 or fold change <0.83;  $P < 0.05$ ). Using the Kyoto Encyclopedia of Genes and Genomes as well as gene ontology analysis, we found that DOX treatment activated the signaling pathways related with P53 signaling and the cell cycle, indicating the successful induction of cardiotoxicity (Fig. 1b and Supplementary Fig. 1). Subsequently, differentially expressed E3 ligases identified by proteomics analysis are listed in Fig. 1c, whereas differentially expressed E3 ligases based on the RNA-seq (GSE40289) analysis are listed in Supplementary Table 3. Regarding the identification of ubiquitination-associated candidate targets, which were consistent in both cell and tissue models, we found that five E3 ligases met the screening criteria, namely TRIM25, CBX4, HERC4, NSMCE2, UBE3C, and ZFP91, among which TRIM25 showed the greatest expression alteration (Fig. 1d and Supplementary Fig. 2).

To explore the role of TRIM25 in the model of DOX-induced cardiotoxicity, primary cultured mouse cardiomyocytes as a well-validated cardiomyocyte model were infected with TRIM25-overexpressing adenovirus (Ad-TRIM25) (MOI 50), confirmed by fluorescent staining, and then treated with DOX (Supplementary Fig. 3). Consistent with previous studies [24, 25], DOX treatment induced substantial apoptosis, as indicated by the increased percentage of terminal dUTP nick-end labeling (TUNEL) positive cells compared with phosphate-buffered saline treatment. Besides, apoptosis-related proteins were also upregulated after DOX treatment. Western blotting confirmed that the levels of pro-apoptosis proteins, such as Bax and cleaved caspase-3, were increased by DOX treatment, whereas that of the anti-apoptosis protein Bcl2 was decreased. Surprisingly, Ad-TRIM25 treatment significantly ameliorated DOX-induced apoptosis (Fig. 1e and Supplementary Fig. 4a, b, c).

Next, we assessed the expression of TRIM25 after treatment with DOX in vitro in a time-dependent manner by western blotting. The early expression of TRIM25 was markedly decreased with a significant increase in Bax levels. Contrastingly, when TRIM25 expression started to increase after 16 h, Bax levels did not increase synchronously (Supplementary Fig. 5). We hypothesized that low TRIM25 expression induced by DOX in the acute phase could have contributed to the cardiotoxicity. TRIM25 expression levels were decreased in both mouse cardiomyocyte HL-1 cells and rat cardiomyocyte H9C2 cells in the acute phase, compared with healthy cells (Figs. 1f, g); this was also verified in heart tissues obtained from mice corresponding to a DOX-induced acute model of cardiotoxicity (Figs. 1f, g).

### TRIM25 is an E3 ligase of p85 $\alpha$

Given that TRIM25 is a ubiquitin E3 ligase, we explored the underlying mechanism of the cardioprotective role of TRIM25 overexpression via immunoprecipitation-mass spectrometry (IP-MS) analysis to identify the specific target. IP-MS demonstrated that the peptide fragment IFEEQCQTQERYSKEYIEK (Supplementary Fig. 6) belonged to p85 $\alpha$  and had ubiquitin modified amino acid residues Gly-Gly in K14 and K19 after transfection with plasmid-Flag-tag-TRIM25 in HL-1 cells, indicating that TRIM25 maybe a ubiquitin E3 ligase for p85 $\alpha$  to promote its ubiquitination and degradation. Furthermore, we also transfected HEK293T cells with plasmid-Flag-p85 $\alpha$ , and the peptide fragment QAGLEAAAK, which belonged to TRIM25, was detected by IP-MS. Co-immunoprecipitation (CO-IP) assays also confirmed this interaction (Supplementary Fig. 7). In light

of negatively correlated protein levels between TRIM25 and p85 $\alpha$  in DOX-induced cardiotoxicity cell-based acute model (Supplementary Fig. 8), we postulated that TRIM25 diminished the DOX-induced cardiotoxicity via the regulation of p85 $\alpha$ .

Next, we further explored whether TRIM25-regulated p85 $\alpha$  stability and protein level via the ubiquitination of p85 $\alpha$ . TRIM25 knockdown by shRNA increased p85 $\alpha$  expression in HL-1 cells (Fig. 2a). Contrastingly, TRIM25 overexpression in both HL-1 and HEK293T cells decreased p85 $\alpha$  expression levels (Fig. 2b and Supplementary Fig. 9). Moreover, we found that TRIM25 overexpression leads to a decrease in p85 $\alpha$  degradation, but that TRIM25 knockdown prolonged p85 $\alpha$  half-life in HEK293T cells (Fig. 2c). Furthermore, overexpression of the loss-of-function mutant TRIM25-2EA (TRIM25 mutant with Glu9 and Glu10 changed to Ala) did not affect the half-life of p85 $\alpha$  (Fig. 2d). CO-IP assays showed that TRIM25 interacts with p85 $\alpha$  endogenously in HL-1 cells (Figs. 2e, f). Moreover, reduced p85 $\alpha$  levels can be rescued by the proteasome inhibitor MG132 (Fig. 2g). P85 $\alpha$  overexpression induced by TRIM25 downregulation could be attenuated by TRIM25 overexpression, indicating that TRIM25 overexpression may induce p85 $\alpha$  degradation (Fig. 2h). Taken together, these results indicated that TRIM25 ubiquitinated p85 $\alpha$  and led to its degradation.

Furthermore, the interaction between endogenous TRIM25 and p85 $\alpha$  was validated in HEK293T cells (Figs. 3a, b). Next, we generated a series of truncated mutants of TRIM25 and p85 $\alpha$  to detect functional domains of the TRIM25-p85 $\alpha$  interaction. Similar to other TRIM family members, TRIM25 contains a cluster of RING, coiled-coil, and PRY/SPRY domains, all of which were constructed in our study. Binding analysis revealed that the PRY/SPRY domain of TRIM25 was bound to p85 $\alpha$  as full-length TRIM25, whereas the RING and CC domains were not (Fig. 3c). Moreover, we found that the SH2 domain of p85 $\alpha$  was crucial for its interaction with TRIM25 (Fig. 3d). Finally, IP-MS demonstrated that the peptide fragment IFEEQCQTQERYSKEYIEK (Supplementary Fig. 6) belonged to p85 $\alpha$  and had ubiquitin modified residues amino acids Gly-Gly in K14 and K19 after transfecting HL-1 cells with Flag-TRIM25, suggesting that TRIM25 might target K506 and K511 of p85 $\alpha$  to promote its ubiquitination and degradation. To verify this hypothesis, we constructed two mutants with Lys506 and Lys511 of p85 $\alpha$  changed into Arg (termed as K506R and K511R). The biochemistry data showed that suppression of the ubiquitination level of p85 $\alpha$  was observed when the p85 $\alpha$ -K506R or K511R mutants were expressed, indicating that TRIM25 targets K506 and K511 of p85 $\alpha$  to promote ubiquitination and degradation (Fig. 3e). Collectively, these data demonstrate that TRIM25 is an E3 ligase of p85 $\alpha$  and can promote its degradation by enhancing its ubiquitination.

Glutathione S-transferase pulldown assays showed that p85 $\alpha$  could interact with TRIM25 (Fig. 3f). Computational molecular docking simulation analyses of the PRY/SPRY domain of TRIM25 to the SH2 domain of p85 $\alpha$ . Eight hydrogen bonding forces revealed the high possibility of combining structures (Fig. 3g).

### TRIM25 inhibits doxorubicin-induced cardiotoxicity

To explore the function of TRIM25 in DOX-induced cardiotoxicity, we used a chronic model by injecting adeno-associated virus 9 (AAV9) expressing TRIM25 (AAV9-TRIM25) into 8-week-old mice via the tail vein. The induction of cardiotoxicity was maintained by a four-week low-dose DOX treatment to simulate the course of clinical chemotherapy (Supplementary Fig. 10a). Cardiomyocyte-specific TRIM25 overexpression (OE) mice were established. Western blotting and quantitative polymerase chain reaction analyses confirmed the efficiency of TRIM25 overexpression in the heart (Supplementary Fig. 10b, c). After DOX administration, no significant differences were observed in body weight between the TRIM25 OE and DOX groups (Supplementary Fig. 11). Echocardiographic assessment revealed a significant diminishment of cardiac

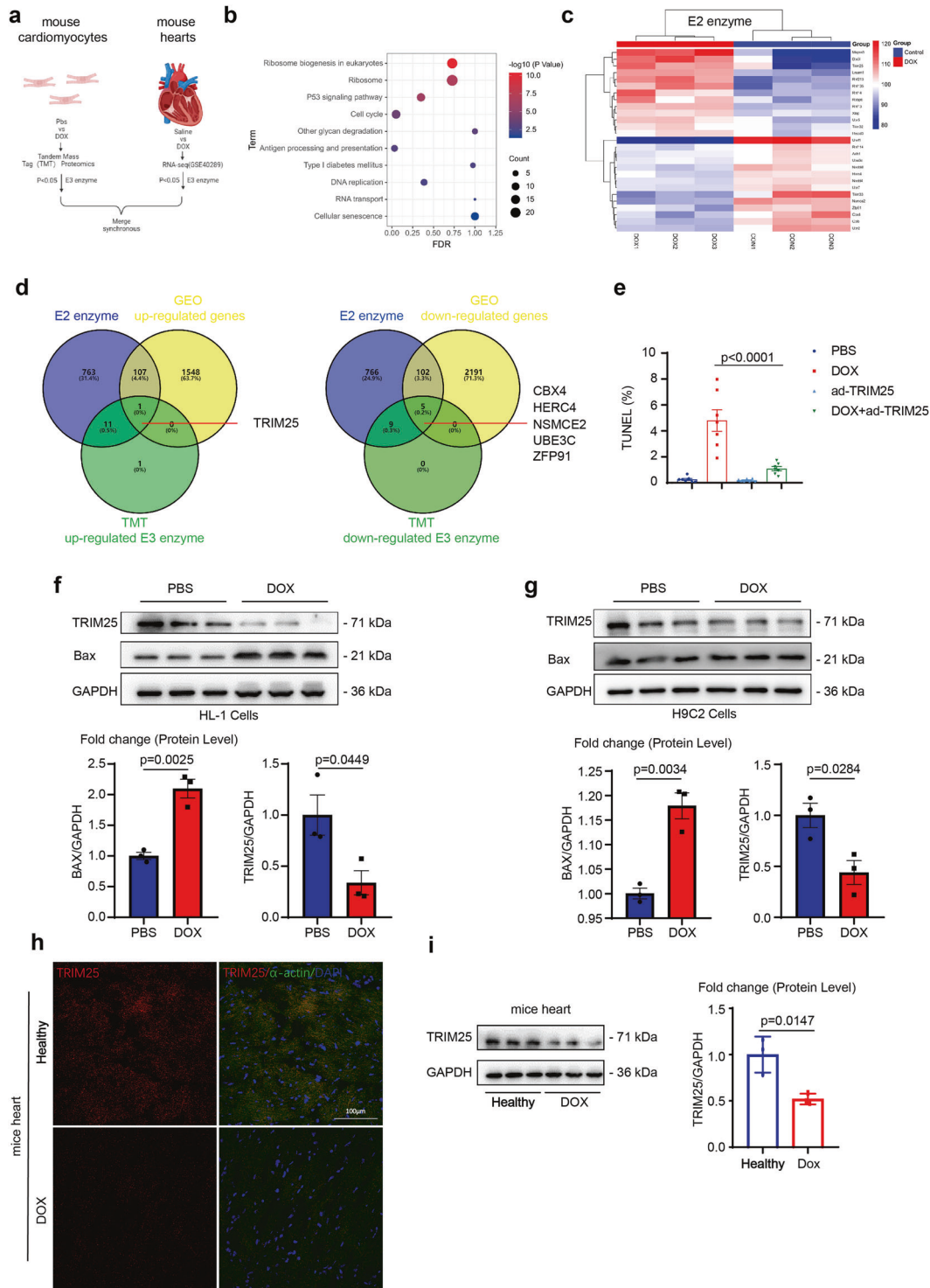


**Fig. 1 Ubiquitin E3 ligase TRIM25 level is decreased in DOX-treated cardiomyocytes.** **a** Scheme showing the procedure of identifying ubiquitination-associated targets in DOX-induced cardiotoxicity. **b** Kyoto Encyclopedia of Genes and Genomes pathway mapping of differentially expressed proteins of DOX-treated cardiomyocytes and control cardiomyocytes. **c** Hierarchical clustering heatmap of the profile of differentially expressed genes from cardiomyocytes between DOX and phosphate-buffered saline hearts. **d** Venn diagram showing differentially expressed ubiquitination-related targets consistent in cell and tissue models. **e** Percentage of TUNEL-positive nuclei in neonatal mouse ventricular myocytes (NMVMs) of each experimental group. **f, g** Western blot analysis of TRIM25 and Bax in HL-1 and H9C2 cells treated by DOX for 6 h. **h** Localization and quantification of TRIM25 (red) in heart sections from mice treated by DOX for 6 h by confocal laser scanning immunofluorescence. The nucleus is labeled by DAPI (blue). **i** Western blot analysis of TRIM25 levels from the hearts of mice treated by DOX for 6 h. Experiments were independently repeated three times. Data are represented as the means  $\pm$  SEM. *P* values were determined by using one-way ANOVA with Bonferroni *post hoc* test (**d**) and unpaired two-tailed Student's *t* test (*n* = 4, C) (*n* = 3, J). Scale bar, 100  $\mu$ m in I. DOX, doxorubicin; CON, control; NS not significant.

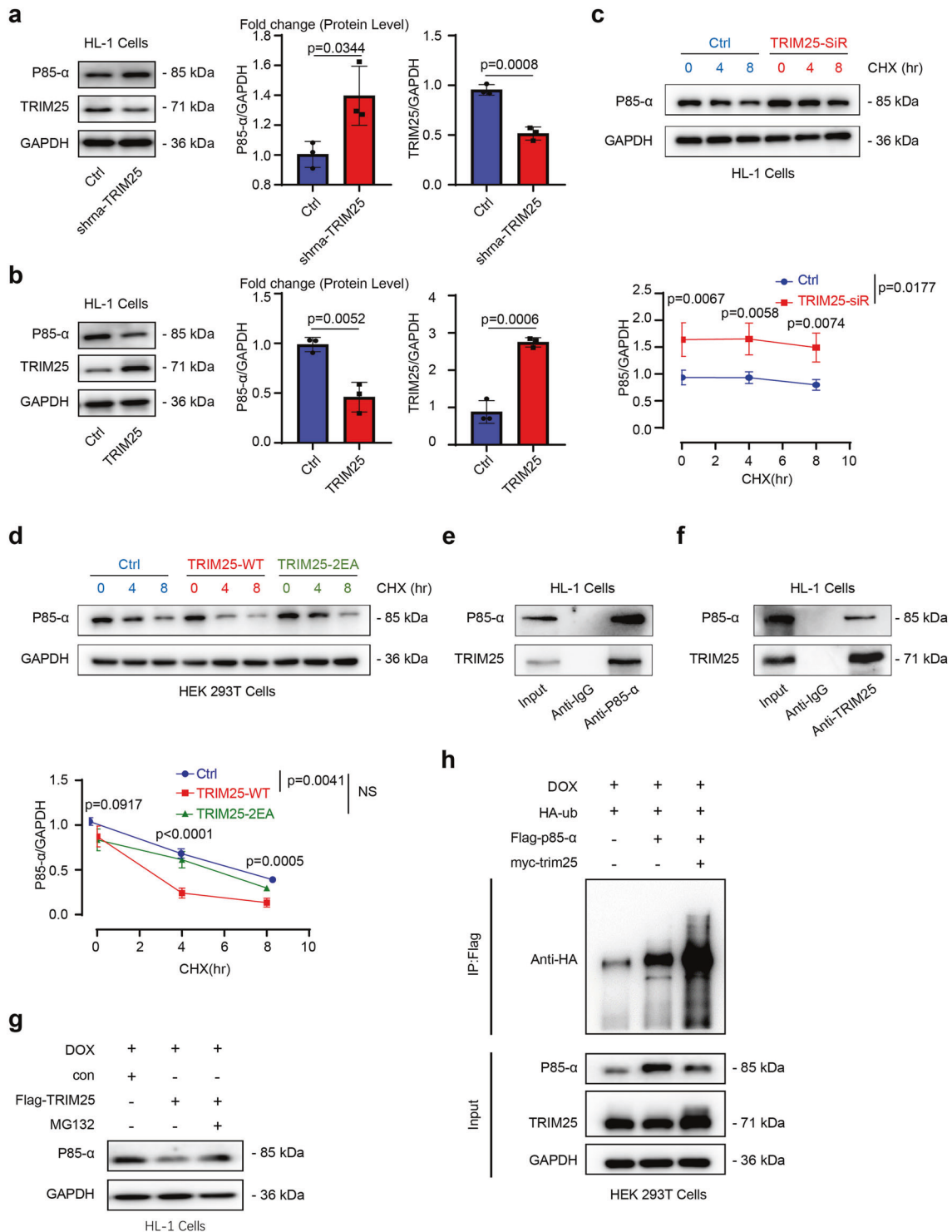


**Fig. 2** TRIM25 decreases p85 $\alpha$  stability via ubiquitination. **a** Western blot analysis of p85 $\alpha$  and TRIM25 levels in HL-1 cells transfected with shRNA-TRIM25 (1  $\mu$ g/ml) or control shRNA. **b** Western blot analysis of p85 $\alpha$  and TRIM25 in HL-1 cells transfected with TRIM25 overexpression plasmids (TRIM25-WT) (1  $\mu$ g/ml) or control plasmid. **c** Representative immunoblot and relative quantification of p85 $\alpha$  in HL-1 transfected with shRNA-TRIM25 or shRNA-Ctrl (1  $\mu$ g/ml), then treated with CHX (100  $\mu$ g/ml) for up to 8 h. **d** Representative immunoblot and relative quantification of p85 $\alpha$  in HL-1 transfected with control plasmid, TRIM25-WT or TRIM25-2EA mutation plasmids (TRIM25-2EA) (1  $\mu$ g/ml), then treated with CHX (100  $\mu$ g/ml) for up to 8 h. **e**, **f** Co-immunoprecipitation (CO-IP) assay analyzed the interaction of endogenous TRIM25 and p85 $\alpha$  in HL-1 cells. **g** Western blotting assessed the level of p85 $\alpha$  in HL-1 cells treated with or without MG132 (20  $\mu$ M) for 12 h. **h** HL-1 cells transfected with the plasmids as indicated and treated with DOX (1  $\mu$ M) for 12 h. Immunoblot analysis of the cell lysates and p85 $\alpha$ -IP with the indicated antibodies. Data represent the means  $\pm$  SEM. ( $n = 3$ ). P values were determined by unpaired 2-tailed Student  $t$  test (**a**, **b**) and two-way ANOVA between multiple groups (**c**, **d**). WT, wild-type; ctrl, control; TRIM25-2EA, TRIM25 mutant with Glu9 and Glu10 changed into Ala.

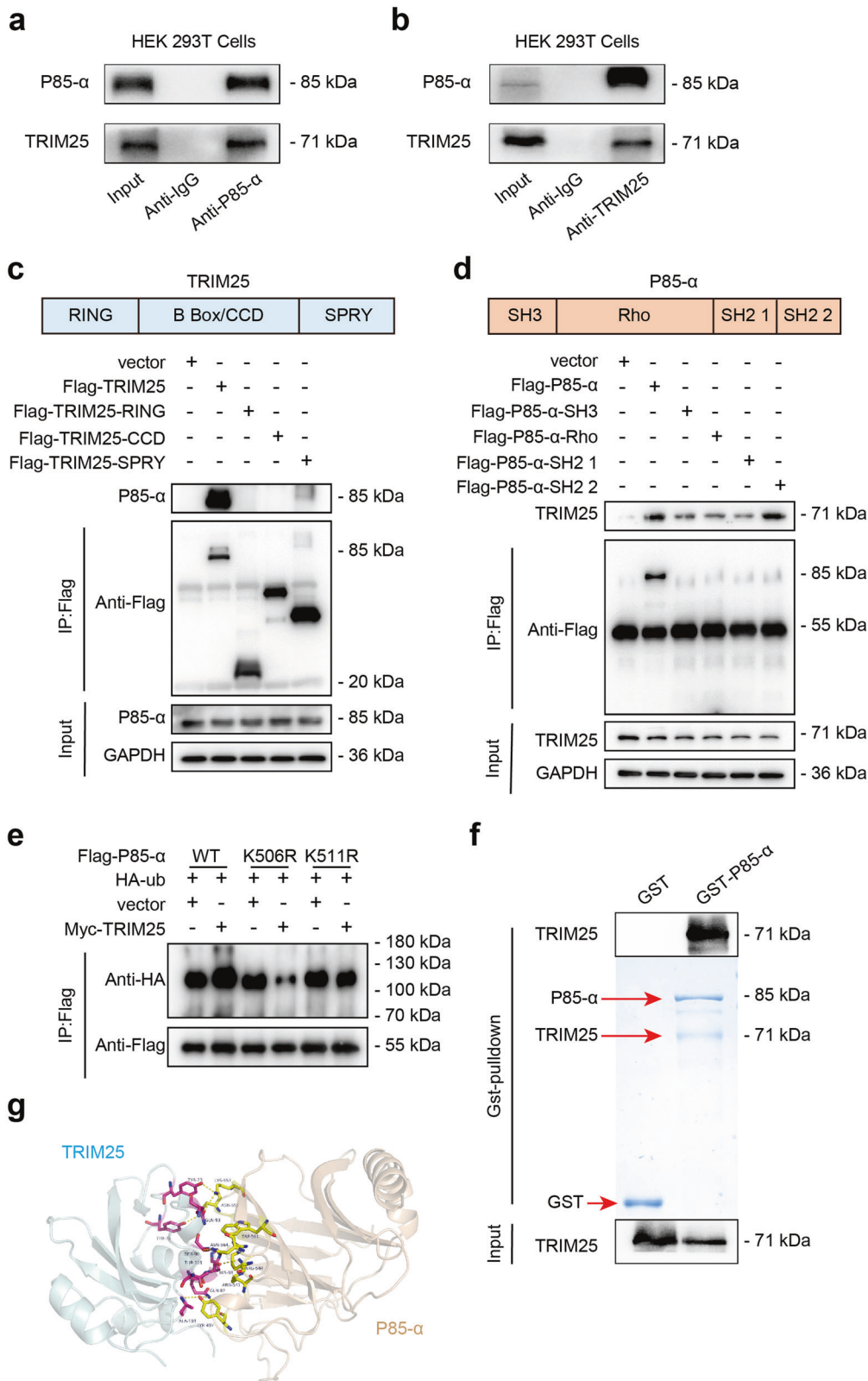


**Fig. 3** TRIM25 interacts and ubiquitinates p85 $\alpha$ . **a, b** CO-IP assay of TRIM25 and p85 $\alpha$  were performed to investigate the interactions between TRIM25 and p85 $\alpha$  in HEK293 cells. **c** HEK293 cells overexpressing full-length and TRIM25 truncates (The RING zinc-finger (R), B-Box/coiled-coil (CC) and SPRY domain of TRIM25) were immunoprecipitated with the indicated antibody. **d** HEK293 cells overexpressing full-length or truncated p85 $\alpha$  were immunoprecipitated with the indicated antibody. **e** Immunoblot analysis of the ubiquitination of wide-type and p85 $\alpha$  mutations (K506R and K511R) with the indicated antibodies. **f** TRIM25 directly binds to p85 $\alpha$ . Glutathione S-transferase (GST)-fused p85 $\alpha$  and His-fused TRIM25 recombinant proteins were co-incubated and subjected to GST pulldown. **g** Computational molecular docking simulation analyses of TRIM25 to p85 $\alpha$ .

contractility and significant upregulation of myocardial atrial natriuretic peptide (Anp) and brain natriuretic peptide (Bnp) mRNA levels in wild-type (WT) mice treated by DOX (Fig. 4a, b, c and Supplementary Table 4). Conversely, the deterioration of left ventricular systolic function as well as the increase of Anp and Bnp mRNA levels were all mitigated in DOX-treated TRIM25 OE mice, demonstrating the protective effects of TRIM25 against DOX-induced cardiotoxicity.

Wasting of cardiomyocytes, fibrosis and apoptosis are acknowledged as key hallmarks in DOX-related cardiotoxicity. DOX-treated TRIM25 OE mice had normal cardiac mass and cardiomyocyte size compared with the WT DOX group (Fig. 4d, e). We found that fibrosis was mitigated in TRIM25 OE mice, as indicated by Masson staining, and that the expression of profibrotic genes in the heart was downregulated (Fig. 4f, g). Moreover, TUNEL staining and the expression of apoptosis proteins, such as Bax and Bcl2, revealed that apoptosis was significantly lower in AAV-TRIM25-DOX than in WT-DOX hearts (Fig. 4h, i).

Given that TRIM25 functions as a feedback mechanism that responds to endoplasmic reticulum (ER) stress, and that the dysregulation of ER homeostasis in the heart is implicated in cardiovascular disease, including DOX cardiomyopathy, we further examined the ER stress-related protein in heart tissues. The expression of BIP/GRP78, a master regulator for ER stress that activates unfolded protein response (UPR) signaling, was increased after treatment with DOX. Activating transcription factor 6 (ATF6), a type II transmembrane protein containing a basic leucine zipper motif, became activated to allow its interaction with ER stress elements and the regulation of the expression of genes encoding BIP and its components. C/EBP homologous protein (CHOP, also known as DDIT3) is a pro-apoptotic mediator. The overexpression of ATF6 and CHOP were downregulated by TRIM25 overexpression (Fig. 4j).

Overall, these results demonstrated that TRIM25 overexpression protects against DOX-induced upregulation of pathways and genes promoting apoptosis, fibrosis, and ER stress.

### TRIM25 mitigates doxorubicin-induced ER stress in cardiomyocytes

To investigate the mechanisms associated with TRIM25-induced cardioprotection, we performed *in vitro* analyses of ER stress, which is considered to be a potential contributor to DOX-induced cardiotoxicity.

We performed transmission electron microscopy to observe the ER lumen in the primary cardiomyocytes treated with DOX. The distention of the ER was augmented by DOX treatment (Fig. 5a), and we found that even a single injection of DOX could result in constant distention of the ER *in vivo* (Supplementary Fig. 12). BIP/GRP78, as sensor and effector for ER stress, is considered as ER stress marker. Western blotting revealed that BIP was elevated in DOX-treated cardiomyocytes and reversed by TRIM25 overexpression. The UPR signaling pathways that govern ER proteostasis, was upregulated by DOX treatment. Additionally, the phosphorylation of JNK pathway was increased after DOX treatment, suggested the maladaptive UPR was also involved in DOX-induced apoptosis (Fig. 5b). Conversely, TRIM25 overexpression attenuated the distention of the ER, as well as the expression of ATF6 and CHOP in DOX-treated cardiomyocytes. The spliced form of XBP-1 (XBP-1s), a crucial transcription factor in mitigating ER stress, was downregulated after DOX treatment. In summary, TRIM25 mitigated DOX-induced ER stress in cardiomyocytes (Fig. 5b, c, d, e). Surprisingly, ATF4, which was elevated in failing hearts in humans, was significantly downregulated in DOX-treated cardiomyocytes and not affected by TRIM25 overexpression (Fig. 5f). ATF4 has pleiotropic functions to reduce the levels of unfolded and misfolded proteins in the ER; however, it can also control CHOP expression to induce cell death. The function of ATF4 in DOX-induced cardiotoxicity needs to be elucidated further in future studies.

### TRIM25 suppresses the UPR by facilitating p85 $\alpha$ degradation

As TRIM25 is a well-known E3 ligase [26], we further investigated whether TRIM25 regulates UPR via the degradation of p85 $\alpha$  specifically. Expectedly, TRIM25 significantly attenuated DOX-induced apoptosis and the protection function of TRIM25 was slightly altered upon p85 $\alpha$  knockdown in the cardiomyocytes (Supplementary Fig. 13). Additionally, TRIM25 significantly decreased ATF6, CHOP, and BIP accumulation in the cardiomyocyte nucleus, whereas XBP-1s was upregulated by TRIM25 (Fig. 6a). Additionally, western blotting revealed that p85 $\alpha$  overexpression markedly reversed the beneficial effect of TRIM25 overexpression on diminishing ER stress, further confirming the therapeutic effect of TRIM25 attributed to the degradation of p85 $\alpha$ .

The regulatory subunits of PI3K, p85 $\alpha$ , and p85 $\beta$  are master regulators of XBP-1s and UPR [27]. As reported, monomers of p85 $\alpha$  and p85 $\beta$  could interact with as well as increase the nuclear translocation of XBP-1s under normal circumstances. To examine the association between p85 $\alpha$  and p85 $\beta$  together with the nuclear translocation of XBP-1s, we increased p85 $\alpha$  input while keeping p85 $\beta$  and XBP-1s expression constant. Western blotting revealed that the nuclear translocation of XBP-1s was reduced when the p85 $\alpha$  expression was increased (Fig. 6b). The immunoprecipitation of the Flag tag decreased XBP-1s expression, confirming an interaction between p85 $\alpha$  and XBP-1s. Furthermore, this interaction was weakened by DOX treatment, which also contributed to further decrease of XBP-1s' nuclear translocation and finally led to ER stress augmentation (Fig. 6c). Immunofluorescence analysis revealed that the expression of p85 $\beta$  was markedly more than that of p85 $\alpha$  in cardiomyocytes. Consistent with the immunofluorescence analysis, western blotting also revealed that DOX treatment resulted in an increase of p85 $\alpha$  while it had no obvious effect on the expression level of p85 $\beta$ . This indicates that after DOX treatment, there was a decrease in the expression of nuclear translocation of XBP-1s (Fig. 6d, e).

### p85 $\alpha$ overexpression or enhanced ER stress in doxorubicin-treated mice abolishes TRIM25-induced cardioprotection

Given that the relationship between ER stress and DOX-induced cardiotoxicity has not been widely explored [28, 29], we examined the role of an anti-ER stress chemical chaperone, tauroursodeoxycholic acid (TUDCA) in DOX-induced cardiomyopathy (Supplementary Fig. 14a). We found that TUDCA could improve heart function and myocardial atrophy significantly (Supplementary Table 5). Moreover, TUDCA strongly decreased Anp and Bnp levels (Supplementary Fig. 14b, c, d, e). Similarly, hematoxylin-eosin staining revealed that the heart's cross-sectional area was improved by TUDCA treatment and Masson staining showed that TUDCA treatment could also decrease the cardiac fibrosis area (Supplementary Fig. 15a, b).

The protective effects of TRIM25 overexpression with respect to DOX-treated cardiotoxicity are likely linked to p85 $\alpha$  downregulation and its role in the UPR. To test this hypothesis, we employed an AAV9 system to overexpress p85 $\alpha$  *in vivo* via tail vein injection. Western blotting and quantitative polymerase chain reaction analyses confirmed p85 $\alpha$  overexpression in the heart of AAV-p85 $\alpha$ -injected mice (Supplementary Fig. 16). As expected, infection with TRIM25 and p85 $\alpha$  significantly blunted the cardioprotective effects of TRIM25 against DOX-induced deterioration of cardiac function (Fig. 7a, b). Similar results were observed when ER stress was enhanced by a pharmacological agent, tunicamycin (TM). AAV-p85 $\alpha$ -injection or TM could impair cardiac contractility (Supplementary Table 6). In the mouse model, cardiac atrophy enhanced by AAV-p85 $\alpha$ -injection or TM was evident in heart weight/tibia length ratios and cardiomyocyte size (Fig. 7c, d). Masson and TUNEL staining illustrated that DOX-induced cardiac fibrosis and apoptosis was increased by AAV-p85 $\alpha$ -injection or TM

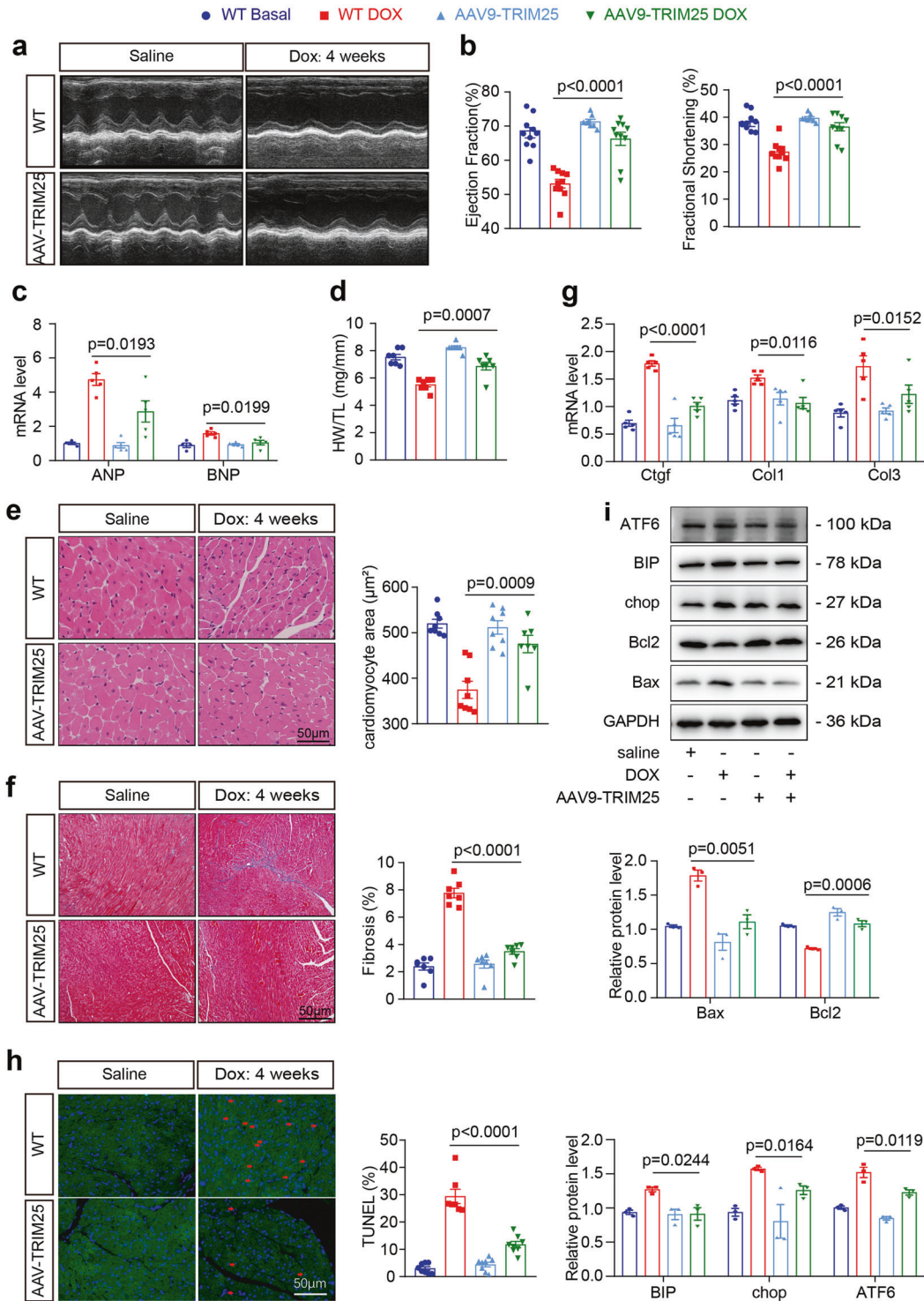


**Fig. 4** TRIM25 overexpression by adeno-associated virus alleviates DOX-induced cardiotoxicity in mice. WT and TRIM25 overexpression (OE) mice were injected by adeno-associated virus 9 via the tail vein, and after 4 weeks, they were treated with a cumulative dose of 20 mg/kg DOX or saline by 4 weekly injections (5 mg/kg on days 0, 7, 14 and 21). **a** Representative M-mode echocardiographic images of WT and AAV-TRIM25 hearts 8 weeks after the first DOX injection. **b** M-mode images from three consecutive cardiac cycles for each animal were used to calculate ventricular measurements: ejection fraction, fractional shortening. **c** Relative quantification of cardiac Anp (atrial natriuretic peptide) and Bnp (brain natriuretic peptide) mRNA expression levels. **d** The HW/TL (heart weight/tibia length) ratio as a cardiac atrophy index of DOX-treated WT and AAV-TRIM25 mice. **e** Representative images of H&E staining and relative quantification of cardiomyocyte area in heart sections from mice treated as in (a). **f, g** Representative images of Masson staining and relative quantification of collagen deposition in heart sections from mice. **h** Representative images of TUNEL staining (left) and quantification of TUNEL-positive nuclei per field (right) in heart sections from WT and AAV-TRIM25 mice treated with DOX or saline. **i** Immunoblot (upper) and relative quantification (lower) of indicated targets in whole hearts from WT and AAV-TRIM25 mice treated as in (a) ( $n = 3$ ).  $N = 7-10$  animals/group; Values represent mean  $\pm$  SEM.  $P$  values were analyzed by one-way ANOVA test with Bonferroni *post hoc* test (b-i). Scale bar, 50  $\mu$ m in e, f and h.

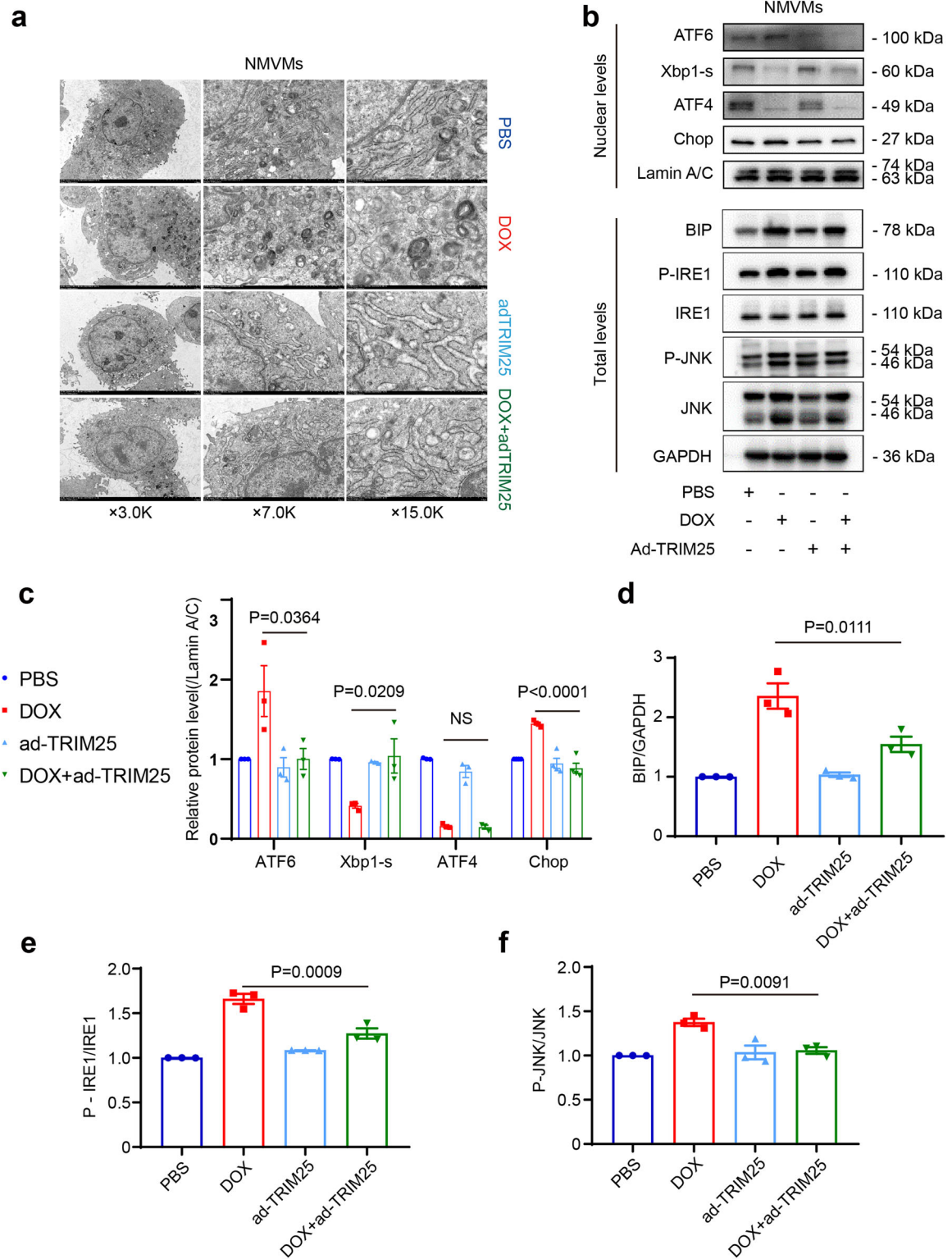


**Fig. 5** TRIM25 overexpression by adenovirus attenuates DOX-induced apoptosis and endoplasmic reticulum stress in cardiomyocytes. **a** DOX-induced NMVMs were transfected with Ad-TRIM25 and assessed by transmission electron microscopy. **b** Representative western blotting (above) and the corresponding quantified graph (c–f) (below) of Atf6, Atf4, XBP1-s, and Chop in the nuclear fraction and BIP, P-IRE1, IRE1, P-JNK, and JNK in the total protein of NMVMs. Data represent the means  $\pm$  SEM ( $n = 3–5$ ). *P* values were analyzed by one-way ANOVA test with Bonferroni *post hoc* test (c, d, e, f). Ad-TRIM25, adenovirus-TRIM25; NS not significant, NMVM neonatal mouse ventricular myocytes.



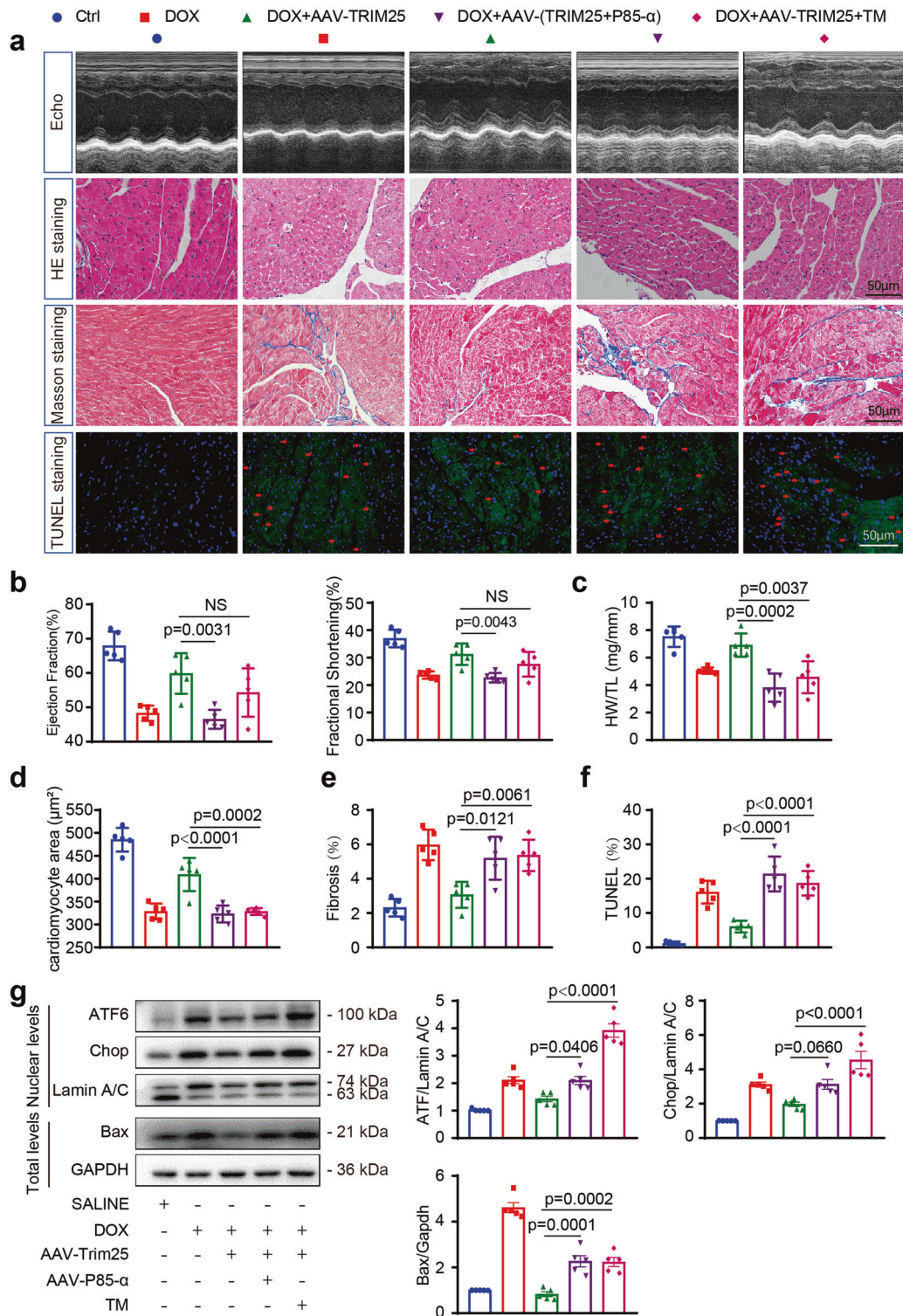


**Fig. 7 Pharmacological augmentation of endoplasmic reticulum stress or p85 $\alpha$  overexpression abolishes cardioprotection in TRIM25 OE mice.** TRIM25 or p85 $\alpha$  overexpression (OE) mice were injected by adeno-associated virus 9 via the tail vein, and after 4 weeks, they were treated with a cumulative dose of 20 mg/kg DOX by 4 weekly injections (5 mg/kg on days 0, 7, 14, and 21) and TM (tunicamycin) (2 mg/kg on days 0, 7, 14, and 21). **a** Representative M-mode echocardiographic images as well as H&E, Masson, and TUNEL staining in heart sections from CON, DOX, AAV-TRIM25, AAV-p85 $\alpha$ , and TM-administered mice. **b** M-mode images from three cardiac cycles for each animal were used to calculate ventricular measurements: ejection fraction, fractional shortening. **c** The HW/TL (heart weight/tibia length) ratio as a cardiac atrophy index of mice. **(d, e, f)** Relative quantification of cardiomyocyte area, fibrosis, and TUNEL-positive nuclei per field in heart sections from CON, DOX, AAV-TRIM25, AAV-p85 $\alpha$ , and TM-administered mice. **g** Nuclear protein amounts of ATF6, CHOP, and Lamin A/C in mice hearts treated with DOX, AAV-TRIM25, AAV-p85 $\alpha$ , and TM. Western blot and relative quantification for Bax in heart tissue from mice infected with DOX, AAV-TRIM25, AAV-p85 $\alpha$ , and TM.  $N = 5$  animals/group; Values represent mean  $\pm$  SEM. Scale bar, 50  $\mu$ m in **a**. TM tunicamycin.

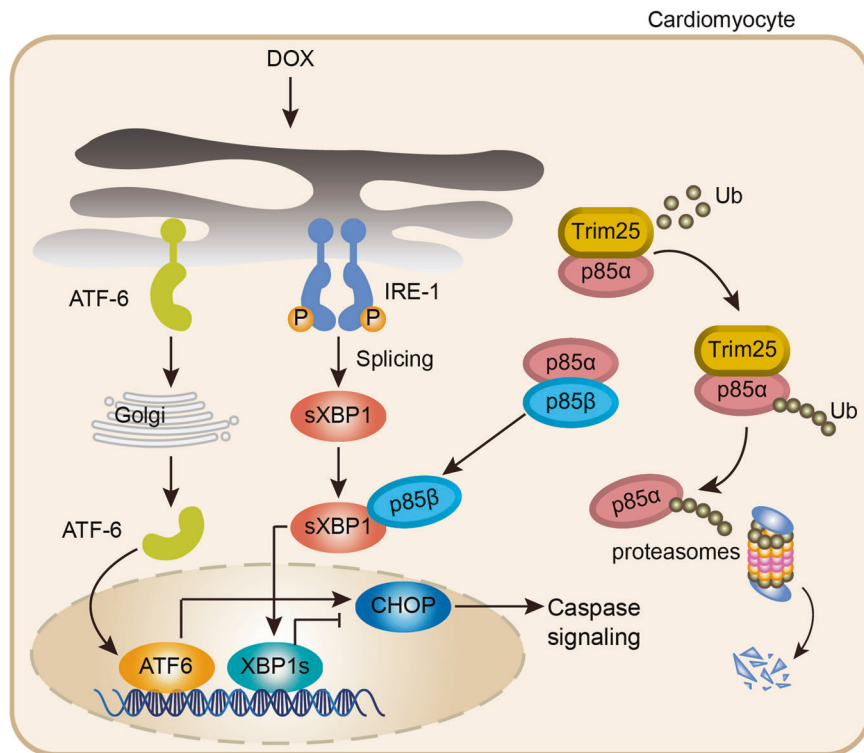


**Fig. 8 Schematic diagram of the molecular mechanisms underlying TRIM25-regulated DOX-induced cardiotoxicity.** A schematic model illustrating that TRIM25 regulates the p85 $\alpha$ /XBP-1s/CHOP signaling pathway under ER stress to decrease myocardial apoptosis. TRIM25, which is downregulated after treatment with DOX, could alleviate ER stress by targeting p85 $\alpha$  for ubiquitination and degradation, leading to increased XBP-1s transferring to the nucleus.

[33]. Wang et al. have reported that a significant decrease in TRIM25 expression at the early stage of doxorubicin treatment and TRIM25 could play a role in the reversal of doxorubicin-induced cardiotoxicity in both *in vivo* and *in vitro* models, which is consistent with our results [34]. In contrast, we treated cardiomyocytes with doxorubicin at a concentration of 1  $\mu$ M, which is closer to the concentration of doxorubicin exposure of cardiomyocytes in clinical chemotherapy, therefore, our results indicated important alterations and effects of endoplasmic reticulum stress in doxorubicin-induced cardiotoxicity. Furthermore, we have found that, as a ubiquitin E3 ligase, TRIM25 participated in degrading p85 $\alpha$  and in turn modified UPR signaling, resulting in the amelioration of cardiomyocyte ER stress and apoptosis.

The role of ER stress in cardiac diseases is vital with respect to multiple pathological developments [19, 35]. Notably, the unique pathological change of DOX-induced ER distention was observed in our study as well as in a previous report by Minotti [36], whereby the distention could last for more than 8 weeks even with a single injection of DOX *in vivo*. Whether this pathological ER change is responsible for the increased long-term cardiac mortality in patients with cancer remains unclear. Furthermore, our findings revealed that DOX augmented ER stress in cardiomyocytes and that this increase is harmful to the heart *in vivo*. Attenuating ER stress via the injection of TUDCA, an anti-ER stress chemical chaperone, is a useful method to prevent DOX-induced cardiomyopathy.

Regarding the accumulation of ER stress, the UPR represents a key adaptive response to regulate improperly folded proteins and restore ER homeostasis [37, 38]. As reported previously, signaling including the protein kinase RNA (PKR)-like ER kinase (PERK)-eukaryotic translation initiation factor 2A (eIF2 $\alpha$ )-activating transcription factor (ATF) 4-C/EBP homologous protein (CHOP) pathway, transcription factor 6 (ATF6)-CHOP pathway, and inositol-requiring kinase 1 (IRE1)-X-box binding protein 1 (XBP1)

pathway control the UPR [39]. Sustained UPR activation can lead to a maladaptive condition and eventually, cell death. In the current study, the nuclear levels of ATF6, XBP-1s, and CHOP revealed the role of UPR in DOX-induced cardiotoxicity. The impaired XBP-1s nuclear translocation induced by DOX may be one of the reasons for maladaptive UPR. Yucel et al. reported that XBP-1s was an important transcription factor in regulating UPR target genes involved in protein folding [40]. XBP-1s nuclear translocation could increase ER-resident protein mesencephalic astrocyte-derived neurotrophic factor transcription and reduce ER stress [41]. Inactivation of mesencephalic astrocyte-derived neurotrophic factor induces cell death by upregulation of the pro-apoptotic mediator, CHOP [42]. A large amount of evidence has indicated the beneficial effect of XBP-1s in cardiovascular diseases. Wang et al. also indicated that XBP-1s expression was reduced in both human and rodent cardiac tissues under heart failure, and that XBP-1s overexpression prevented the development of cardiac dysfunction [43]. Furthermore, XBP-1s couples the UPR to the HBP (hexosamine biosynthetic pathway) to protect cells under stress, which protect the heart from ischemia/reperfusion damage [44, 45]. Interestingly, our study and a previous study by Park et al. showed that monomers of p85 $\alpha$  or p85 $\beta$  could increase the nuclear translocation of the spliced XBP-1 separately [27]. However, another study suggested that there was a competitive interaction among p85 $\alpha$ , p85 $\beta$ , and XBP-1s under normal circumstances, whereby p85 $\alpha$  and p85 $\beta$  form heterodimers. However, the homeostasis among p85 $\alpha$ , p85 $\beta$ , and XBP-1s was broken by the expression of E3 enzyme which regulated the expression level of p85 $\alpha$ , p85 $\beta$ , and XBP-1s induced by DOX. Our data also demonstrated that DOX could further decrease the transport of XBP-1s by decreasing the interaction between p85 $\alpha$  and XBP-1s. Previous research has shown that there is a reduced accumulation of UPR proteins such as BIP (the hallmark of ER stress), CHOP, and ATF6 in the absence of p85 $\alpha$  in fibroblasts

treated with tunicamycin [46]. In our study, the therapeutic effect of TRIM25 overexpression, would be attributable, at least in part, to p85 $\alpha$  downregulation.

In summary, our study provides evidence that TRIM25 mediated DOX induced ER stress via its effects on the p85 $\alpha$ -XBP-1s pathway. Our findings, therefore, highlight a novel role of TRIM25 in DOX-induced cardiotoxicity. Targeting the p85 $\alpha$ -XBP-1s pathway by regulating the ubiquitin E3 ligase, TRIM25, may provide a potential strategy for patients undergoing chemotherapy-based regimens.

## DATA AVAILABILITY

The data in the study are available upon reasonable request.

## REFERENCES

- Li M, Sala V, De Santis MC, Cimino J, Cappello P, Pianca N, et al. Phosphoinositide 3-Kinase Gamma Inhibition Protects From Anthracycline Cardiotoxicity and Reduces Tumor Growth. *Circulation*. 2018;138:696–711.
- Shen Y, Zhang H, Zhang Q, Zhang B, Ni Y, Zhao R, et al. Right Ventricular Ejection Fraction Assessed by Three-Dimensional Echocardiography Is Associated with Long-Term Adverse Clinical Cardiac Events in Patients with Anthracycline-Induced Cardiotoxicity. *J Am Soc Echocardiogr*. 2022;35:600–8.
- de Vries S, Schaapveld M, Janus CPM, Daniels LA, Petersen EJ, van der Maazen RWM, et al. Long-Term Cause-Specific Mortality in Hodgkin Lymphoma Patients. *J Natl Cancer Inst*. 2021;113:760–9.
- Zhang S, Liu X, Bawa-Khalife T, Lu LS, Lyu YL, Liu LF, et al. Identification of the molecular basis of doxorubicin-induced cardiotoxicity. *Nat Med*. 2012;18:1639–42.
- Burridge PW, Li YF, Matsa E, Wu H, Ong SG, Sharma A, et al. Human induced pluripotent stem cell-derived cardiomyocytes recapitulate the predilection of breast cancer patients to doxorubicin-induced cardiotoxicity. *Nat Med*. 2016;22:547–56.
- Willis MS, Townley-Tilson WH, Kang EY, Homeister JW, Patterson C. Sent to destroy: the ubiquitin proteasome system regulates cell signaling and protein quality control in cardiovascular development and disease. *Circ Res*. 2010;106:463–78.
- Pagan J, Seto T, Pagano M, Cittadini A. Role of the ubiquitin proteasome system in the heart. *Circ Res*. 2013;112:1046–58.
- Glickman MH, Ciechanover A. The ubiquitin-proteasome proteolytic pathway: destruction for the sake of construction. *Physiol Rev*. 2002;82:373–428.
- Hershko A. The ubiquitin system for protein degradation and some of its roles in the control of the cell-division cycle (Nobel lecture). *Angew Chem Int Ed Engl*. 2005;44:5932–43.
- Zhao D, Zhong G, Li J, Pan J, Zhao Y, Song H, et al. Targeting E3 Ubiquitin Ligase WWP1 Prevents Cardiac Hypertrophy Through Destabilizing DVL2 via Inhibition of K27-Linked Ubiquitination. *Circulation*. 2021;144:694–711.
- Shen H, Zhang J, Wang C, Jain PP, Xiong M, Shi X, et al. MDM2-Mediated Ubiquitination of Angiotensin-Converting Enzyme 2 Contributes to the Development of Pulmonary Arterial Hypertension. *Circulation*. 2020;142:1190–204.
- Wang Y, Han D, Zhou T, Chen C, Cao H, Zhang JZ, et al. DUSP26 induces aortic valve calcification by antagonizing MDM2-mediated ubiquitination of DPP4 in human valvular interstitial cells. *Eur Heart J*. 2021;42:2935–51.
- Ranek MJ, Wang X. Activation of the ubiquitin-proteasome system in doxorubicin cardiomyopathy. *Curr Hypertens Rep*. 2009;11:389–95.
- Fan GC, Zhou X, Wang X, Song G, Qian J, Nicolaou P, et al. Heat shock protein 20 interacting with phosphorylated Akt reduces doxorubicin-triggered oxidative stress and cardiotoxicity. *Circ Res*. 2008;103:1270–9.
- Kedar V, McDonough H, Arya R, Li HH, Rockman HA, Patterson C. Muscle-specific RING finger 1 is a bona fide ubiquitin ligase that degrades cardiac troponin I. *Proc Natl Acad Sci*. 2004;101:18135–40.
- Li Y, Wu H, Wu W, Zhuo W, Liu W, Zhang Y, et al. Structural insights into the TRIM family of ubiquitin E3 ligases. *Cell Res*. 2014;24:762–5.
- Wang L, Zhang X, Lin ZB, Yang PJ, Xu H, Duan JL, et al. Tripartite motif 16 ameliorates nonalcoholic steatohepatitis by promoting the degradation of phospho-TAK1. *Cell Metab*. 2021;33:1372–88.
- Gack MU, Shin YC, Joo CH, Urano T, Liang C, Sun L, et al. TRIM25 RING-finger E3 ubiquitin ligase is essential for RIG-I-mediated antiviral activity. *Nature*. 2007;446:916–20.
- Binder P, Wang S, Radu M, Zin M, Collins L, Khan S, et al. Pak2 as a Novel Therapeutic Target for Cardioprotective Endoplasmic Reticulum Stress Response. *Circ Res*. 2019;124:696–711.
- Tang X, Pan L, Zhao S, Dai F, Chao M, Jiang H, et al. SNO-MLP (S-Nitrosylation of Muscle LIM Protein) Facilitates Myocardial Hypertrophy Through TLR3 (Toll-Like Receptor 3)-Mediated RIP3 (Receptor-Interacting Protein Kinase 3) and NLRP3 (NOD-Like Receptor Pyrin Domain Containing 3) Inflammasome Activation. *Circulation*. 2020;141:984–1000.
- Ge Z, Leighton JS, Wang Y, Peng X, Chen Z, Chen H, et al. Integrated Genomic Analysis of the Ubiquitin Pathway across Cancer Types. *Cell Rep*. 2018;23:213–26. e3.
- Li C, Han T, Li Q, Zhang M, Guo R, Yang Y, et al. MKRN3-mediated ubiquitination of Poly(A)-binding proteins modulates the stability and translation of GNRH1 mRNA in mammalian puberty. *Nucl Acids Res*. 2021;49:3796–813.
- Ni Y, Xu Z, Li C, Zhu Y, Liu R, Zhang F, et al. Therapeutic inhibition of miR-802 protects against obesity through AMPK-mediated regulation of hepatic lipid metabolism. *Theranostics*. 2021;11:1079–99.
- Han D, Wang Y, Wang Y, Dai X, Zhou T, Chen J, et al. The Tumor-Suppressive Human Circular RNA CircITCH Sponges miR-330-5p to Ameliorate Doxorubicin-Induced Cardiotoxicity Through Upregulating SIRT6, Survivin, and SERCA2a. *Circ Res*. 2020;127:e108–e25.
- Russo M, Guida F, Paparo L, Trinchese G, Aitoro R, Avagliano C, et al. The novel butyrate derivative phenylalanine-butyramide protects from doxorubicin-induced cardiotoxicity. *Eur J Heart Fail*. 2019;21:519–28.
- Koliopoulos MG, Esposito D, Christodoulou E, Taylor IA, Rittinger K. Functional role of TRIM E3 ligase oligomerization and regulation of catalytic activity. *EMBO J*. 2016;35:1204–18.
- Park SW, Zhou Y, Lee J, Lu A, Sun C, Chung J, et al. The regulatory subunits of PI3K, p85 $\alpha$  and p85 $\beta$ , interact with XBP-1 and increase its nuclear translocation. *Nat Med*. 2010;16:429–37.
- Qiu LZ, Yue LX, Ni YH, Zhou W, Huang CS, Deng HF, et al. Emodin-Induced Oxidative Inhibition of Mitochondrial Function Assists BiP/IRE1 $\alpha$ /CHOP Signaling-Mediated ER-Related Apoptosis. *Oxid Med Cell Longev*. 2021;2021:8865813.
- Yarmohammadi F, Rezaee R, Haye AW, Karimi G. Endoplasmic reticulum stress in doxorubicin-induced cardiotoxicity may be therapeutically targeted by natural and chemical compounds: A review. *Pharm Res*. 2021;164:105383.
- Tocchetti CG, Carpi A, Coppola C, Quintavalle C, Rea D, Campesan M, et al. Ranolazine protects from doxorubicin-induced oxidative stress and cardiac dysfunction. *Eur J Heart Fail*. 2014;16:358–66.
- Lipshultz SE, Scully RE, Lipsitz SR, Sallan SE, Silverman LB, Miller TL, et al. Assessment of dexrazoxane as a cardioprotectant in doxorubicin-treated children with high-risk acute lymphoblastic leukaemia: long-term follow-up of a prospective, randomised, multicentre trial. *Lancet Oncol*. 2010;11:950–61.
- Liu J, Zheng H, Tang M, Ryu YC, Wang X. A therapeutic dose of doxorubicin activates ubiquitin-proteasome system-mediated proteolysis by acting on both the ubiquitination apparatus and proteasome. *Am J Physiol Heart Circ Physiol*. 2008;295:H2541–50.
- Liu Y, Tao S, Liao L, Li Y, Li H, Li Z, et al. TRIM25 promotes the cell survival and growth of hepatocellular carcinoma through targeting Keap1-Nrf2 pathway. *Nat Commun*. 2020;11:348.
- Wang X, Lian Z, Ge Y, Yu D, Li S, Tan K. TRIM25 Rescues Against Doxorubicin-Induced Pyroptosis Through Promoting NLRP1 Ubiquitination. *Cardiovasc Toxicol*. 2021;21:859–68.
- Blackwood EA, Azizi K, Thuerauf DJ, Paxman RJ, Plate L, Kelly JW, et al. Pharmacologic ATF6 activation confers global protection in widespread disease models by reprogramming cellular proteostasis. *Nat Commun*. 2019;10:187.
- Minotti G, Menna P, Salvatorelli E, Cairo G, Gianni L. Anthracyclines: molecular advances and pharmacologic developments in antitumor activity and cardiotoxicity. *Pharm Rev*. 2004;56:185–229.
- Ron D, Walter P. Signal integration in the endoplasmic reticulum unfolded protein response. *Nat Rev Mol Cell Biol*. 2007;8:519–29.
- Minamino T, Komuro I, Kitakaze M. Endoplasmic reticulum stress as a therapeutic target in cardiovascular disease. *Circ Res*. 2010;107:1071–82.
- Hetz C, Zhang K, Kaufman RJ. Mechanisms, regulation and functions of the unfolded protein response. *Nat Rev Mol Cell Biol*. 2020;21:421–38.
- Yucel SS, Stelzer W, Lorenzoni A, Wozny M, Langosch D, Lemberg MK. The Metastable XBP1u Transmembrane Domain Defines Determinants for Intramembrane Proteolysis by Signal Peptide Peptidase. *Cell Rep*. 2019;26:3087–99. e11.
- Wang D, Hou C, Cao Y, Cheng Q, Zhang L, Li H, et al. XBP1 activation enhances MANF expression via binding to endoplasmic reticulum stress response elements within MANF promoter region in hepatitis B. *Int J Biochem Cell Biol*. 2018;99:140–6.
- Herranen A, Ikaheimo K, Lankinen T, Pakarinen E, Fritzsche B, Saarna M, et al. Deficiency of the ER-stress-regulator MANF triggers progressive outer hair cell death and hearing loss. *Cell Death Dis*. 2020;11:100.
- Wang X, Deng Y, Zhang G, Li C, Ding G, May HI, et al. Spliced X-box Binding Protein 1 Stimulates Adaptive Growth Through Activation of mTOR. *Circulation*. 2019;140:566–79.
- Wang ZV, Deng Y, Gao N, Pedrozo Z, Li DL, Morales CR, et al. Spliced X-box binding protein 1 couples the unfolded protein response to hexosamine biosynthetic pathway. *Cell*. 2014;156:1179–92.

45. Glembotski CC. Finding the missing link between the unfolded protein response and O-GlcNAcylation in the heart. *Circ Res.* 2014;115:546–8.
46. Winnay JN, Boucher J, Mori MA, Ueki K, Kahn CR. A regulatory subunit of phosphoinositide 3-kinase increases the nuclear accumulation of X-box-binding protein-1 to modulate the unfolded protein response. *Nat Med.* 2010;16:438–45.

### ACKNOWLEDGEMENTS

We gratefully acknowledge Zhiyuan Zhang in the department of General Surgery at Zhongshan Hospital for ubiquitination-associated technical advice and help. This study was supported by the National Natural Science Foundation of China (No. 81771840, 82170359), Clinical Research Project of Zhongshan Hospital (No.2020ZSLC21), and Smart Medical Treatment Project of Zhongshan Hospital (No.2020ZH516).

### AUTHOR CONTRIBUTIONS

LC and YS conceived the study. JZ designed the experiments. YS, HZ, YN, XW, YC, JC, YW, JL, and YX performed the experiments and analyzed the data. YS wrote the initial draft of article. LC and JZ revised the article. All authors approved the final version of the manuscript.

### COMPETING INTERESTS

The authors declare no competing interests.

### ETHICS APPROVAL AND CONSENT TO PARTICIPATE

Our studies did not include human participants, human data or human tissues. All animal experiments conducted were compliant with Ethics Committee of Zhongshan Hospital Research Ethics (2019-09).

### ADDITIONAL INFORMATION

**Supplementary information** The online version contains supplementary material available at <https://doi.org/10.1038/s41419-022-05100-4>.

**Correspondence** and requests for materials should be addressed to Jian-Yuan Zhao or Leilei Cheng.

**Reprints and permission information** is available at <http://www.nature.com/reprints>

**Publisher's note** Springer Nature remains neutral with regard to jurisdictional claims in published maps and institutional affiliations.



**Open Access** This article is licensed under a Creative Commons Attribution 4.0 International License, which permits use, sharing, adaptation, distribution and reproduction in any medium or format, as long as you give appropriate credit to the original author(s) and the source, provide a link to the Creative Commons license, and indicate if changes were made. The images or other third party material in this article are included in the article's Creative Commons license, unless indicated otherwise in a credit line to the material. If material is not included in the article's Creative Commons license and your intended use is not permitted by statutory regulation or exceeds the permitted use, you will need to obtain permission directly from the copyright holder. To view a copy of this license, visit <http://creativecommons.org/licenses/by/4.0/>.

© The Author(s) 2022